RESEARCH MEMORANDUM

A PRELIMINARY INVESTIGATION OF THE STATIC STABILITY CHARACTERISTICS OF FOUR AIRPLANE-LIKE CONFIGURATIONS AT MACH NUMBERS FROM 3.00 TO 6.28

By Thomas J. Wong and Hermilo R. Gloria

Ames Aeronautical Laboratory
Moffett Field, Calif.

NATIONAL ADVISORY COMMITTEE
FOR AERONAUTICS

WASHINGTON
March 26, 1956

NACA RM A56A06

NATIONAL ADVISORY COMMITTEE FOR AERONAUTICS

RESEARCH MEMORANDUM

A PRELIMINARY INVESTIGATION OF THE STATIC STABILITY CHARACTERISTICS OF FOUR AIRPLANE-LIKE CONFIGURATIONS AT MACH NUMBERS FROM 3.00 TO 6.28

By Thomas J. Wong and Hermilo R. Gloria

SUMMARY

Side-force and directional-stability characteristics of four airplane-like configurations were determined at Mach numbers from 3.00 to 6.28, zero angle of attack, and angles of sideslip up to 4°. Two configurations had trapezoidal wing and tail surfaces and two had triangular wing and tail surfaces. Lift, drag, and pitching-moment data were also obtained for the triangular-wing configuration with a conical base flare at angles of attack up to 13°. (These data had been obtained previously for the other configurations.)

In general, it was found that the directional stability of the configurations decreased with increasing Mach number. An increase in the nose fineness ratio of the trapezoidal-wing configuration decreased directional stability. The addition of a conical flare at the base of the triangular-wing configuration increased directional stability. Addition of the flare also increased longitudinal stability as well as lift and drag. Lift-drag ratios were, however, reduced by the addition of the flare.

INTRODUCTION

References 1 through 4 present data for an airplane-like configuration at high supersonic speeds. This configuration consisted of trapezoidal wing and tail surfaces mounted on a cylindrical body which had a fineness-ratio-3 ogival nose. Leading edges of the planar surfaces were blunt as would be required in flight to alleviate local aerodynamic heating. Lift, drag, and static longitudinal and lateral stability data were obtained at Mach numbers of 4.06 and 6.86. A similar configuration was investigated

in reference 5 together with several changes in the basic configuration which were made in an attempt to increase lift-drag ratios. Specifically, triangular-plan-form wing and tail surfaces were employed to permit an increase in leading-edge sweep and thereby a reduction in the drag associated with leading-edge bluntness. A body nose with fineness ratio increased to 5 and with a minimum-drag profile was also employed. Lift, drag, and static longitudinal stability data were obtained at Mach numbers from 3.00 to 6.28. However, no directional-stability data were presented in reference 5. These data have been obtained and are presented herein.

In addition, it was noted in reference 5 that the stability of the configurations decreased with increasing Mach number. This decrease is associated, of course, with the characteristic loss in lift effectiveness of thin planar tail surfaces at high supersonic speeds. It was suggested in reference 1 that the use of tail surfaces with relatively thick wedge sections would increase tail effectiveness at high Mach numbers (see ref. 6). Alternately, it was suggested in reference 5 that the use of a conical base flare on the body would also provide increased stability (see ref. 7). This latter suggestion was studied by adding a conical base flare to one of the models tested in reference 5. The effect of the conical flare on the lift and drag as well as the stability characteristics of the model was determined.

NOTATION

b wing span

C_A axial-force coefficient, $\frac{\text{axial force}}{qS}$

C_D drag coefficient, $\frac{\text{drag}}{qS}$

C_L lift coefficient, $\frac{\text{lift}}{qS}$

C_m pitching-moment coefficient, $\frac{\text{pitching moment about centroid of wing plan area}}{qS\bar{c}}$

C_n yawing-moment coefficient referred to body axes, $\frac{\text{yawing moment about centroid of wing plan area}}{qSb}$

C_Y side-force coefficient, $\frac{\text{side force}}{qS}$

$\bar{c}$ mean aerodynamic chord of wing, including portion submerged in fuselage

f fineness ratio, ratio of body length to body diameter

M free-stream Mach number

q free-stream dynamic pressure

S wing plan-form area, including portion submerged in fuselage

x_{cp} longitudinal center of pressure location, percent $\bar{c}$ from centroid of wing plan-form area, positive forward

α angle of attack, deg

β angle of sideslip, deg

Subscript

β $\frac{\partial}{\partial \beta}$, per deg

APPARATUS AND TESTS

Tests were conducted in the Ames 10- by 14-inch supersonic wind tunnel, which is described in detail in reference 8. Aerodynamic forces and moments acting on the models were measured with a strain-gage balance. All models were sting-supported from the rear. The sting supports were shrouded to within 0.04 inch of the model bases, thereby eliminating, for all practical purposes, aerodynamic loads on the stings.

Base pressures were measured in all tests and the resultant base force (referred to free-stream static pressure) was substracted from the measured total forces. Thus, all data presented represent forces acting on the models ahead of the base.

The principle dimensions of the test configurations are shown in figures 1 and 2. A detailed description of the models may also be found in reference 5. Two basic and two modified configurations were tested. One basic configuration is the trapezoidal wing model shown in figure 1. This model was modified, as indicated by the dashed lines, by replacing

[redacted]

the fineness-ratio-3 ogival nose section with a fineness-ratio-5 minimum-drag nose section (see ref. 5). The other basic configuration is the triangular-wing model shown in figure 2. This model was modified, as indicated by the dashed lines, by adding a conical flare at the base. The flare is the frustum of a fineness-ratio-5 cone extending 2.07 body diameters forward of the base and increasing the body base diameter by $\sqrt{2}$. All models were constructed of steel.

Tests were conducted at Mach numbers of 3.00, 4.26, 5.04, and 6.28, angles of sideslip up to 4°, and angles of attack up to 13°. The free-stream Reynolds numbers based on the length of the models were

Mach number	Reynolds number, million	
	Model with fineness-ratio-3 nose	Models with fineness-ratio-5 nose
3.00	7.5	9.1
4.26	6.9	8.3
5.04	3.3	4.0
6.28	1.4	1.7

In the region of the wind-tunnel test section where the models were located, the variation in stream Mach number did not exceed ±0.02 at Mach numbers from 3.00 to 5.04 and ±0.04 at Mach number 6.28. Deviations in free-stream Reynolds number from the values previously given did not exceed ±100,000. The estimated errors in angle of attack and angle of sideslip did not exceed ±0.2°.

Precision of the data is affected by uncertainties in measurement of forces, moments, and base pressures and in the determination of free-stream dynamic pressure and angle of attack or sideslip. These uncertainties result in maximum possible errors in the aerodynamic force and moment coefficients as shown in the following table.

Mach number	C_D	C_L, C_Y	C_m	C_n
3.00	±0.002	±0.002	±0.004	±0.0005
4.26	±.002	±.002	±.004	±.0005
5.04	±.002	±.002	±.004	±.0005
6.28	±.004	±.004	±.008	±.001

It should be noted that, for the most part, the experimental results presented herein are in error by less than these estimates.

RESULTS AND DISCUSSION

Results of the tests of the four airplane-like configurations are presented in table I, where axial-force, side-force, and yawing-moment coefficients are tabulated for various angles of sideslip and test Mach numbers. In addition, lift, drag, and pitching-moment coefficients, and center-of-pressure locations are presented in table II for the triangular-wing model with base flare at various angles of attack. For the other three test configurations, data corresponding to that given in table II may be found in reference 5. Portions of the data contained in tables I and II will also be presented in graphical form.

In figure 3, the variation of side-force and yawing-moment coefficients with angle of sideslip are presented for the four test configurations at zero angle of attack. It can be seen that, within the limited sideslip-angle range of the tests, the variations in side-force coefficient are, in general, essentially linear for all test Mach numbers and configurations. However, the variations of yawing-moment coefficient are essentially linear only at the lowest test Mach number, 3.00.

Perhaps the most significant trend to be noted in figure 3 is the decrease in slope at $\beta = 0^\circ$ of both the C_n and C_Y curves with increasing Mach number. This point is more clearly illustrated in figure 4 where the directional-stability derivative, C_{n_β} (measured at $\alpha = \beta = 0^\circ$), is shown as a function of Mach number for the four test configurations. Here it is noted that with but one exception, C_{n_β} decreases with increasing Mach number for all configurations. This decrease is a result of the previously noted decrease in effectiveness of the vertical tail.

It may also be noted in figure 4 that modifying the trapezoidal-wing model by replacement of the $f = 3$ nose section with one of $f = 5$ had a destabilizing effect. The decrement in C_{n_β} generally increases with increasing Mach number. Modifying the triangular-wing model by addition of the conical flare had a stabilizing effect. In this case the increment in C_{n_β} was essentially independent of Mach number up to $M = 5.04$. However, the increment increased at $M = 6.28$ so that the stability of the triangular-wing model with base flare remained essentially constant as Mach number increased from 5.04 to 6.28.

It is indicated, therefore, that the stabilizing effectiveness of the conical flare increased at $M = 6.28$. It is believed that this increase can be associated with effects of boundary-layer separation ahead of the tail cone, due, in part, to the relatively low test Reynolds number at $M = 6.28$. The indicated increase in stabilizing effectiveness of the flare may not occur for full-scale Reynolds numbers. A similar trend was observed in reference 9 in tests of a cone-cylinder with a base

flare. (It may also be distinguished in the data of ref. 7.) While the increase in flare effectiveness noted in reference 9 was far greater than that indicated in figure 4, it should be noted that the flare employed was also much larger.

It has been shown that addition of the conical base flare increases the directional stability of the triangular-wing model. It remains now to investigate the effects of the flare on the lift, drag, and pitching-moment characteristics of the model. These effects are illustrated in figures 5 and 6. Lift coefficients as a function of drag coefficients, pitching-moment coefficients, and lift-drag ratios are shown in figure 5 for the triangular-wing models with and without base flare. Lift coefficients as a function of angle of attack are shown in figure 6.

The data for the basic triangular-wing model were taken from reference 5. It is apparent in figure 5 that the addition of the conical flare also increases the longitudinal stability of the model. The modification also increases the drag, however, and while the lift is increased as well (see fig. 6), there is a net reduction in lift-drag ratio. This point is more clearly evident in figure 7 where maximum lift-drag ratios for all four test configurations are shown as a function of test Mach number. The data for all but the triangular-wing model with base flare were taken from reference 5. It may be noted that the addition of the base flare reduces the maximum lift-drag ratios of the triangular-wing model at all Mach numbers. However, the maximum lift-drag ratios obtained for the triangular-wing model with base flare are higher than those obtained for the basic trapezoidal-wing model. It may also be noted that the triangular-wing model with base flare is more stable (see fig. 4). It is apparent that stability about the same as that of the basic trapezoidal-wing model and greater maximum lift-drag ratios could have been achieved with a smaller base flare.

It can also be observed in figure 7 that the maximum lift-drag ratio for all models decreases markedly as the test Mach number is increased from 4.26 to 6.28. This decrease in maximum lift-drag ratio with increasing Mach number is due primarily to the increased skin-friction drag associated with the decrease of test Reynolds number (see, e.g., refs. 5 and 10).

CONCLUSIONS

The static directional stability characteristics of four airplane-like configurations have been determined at Mach numbers from 3.00 to 6.28, zero angle of attack, and angles of sideslip up to 4°. Lift, drag, and pitching-moment data were also obtained for one configuration at angles of

attack up to 13°. (These data had been obtained previously for the other configurations.) From the results of these tests, the following conclusions have been drawn:

1. In general, the directional stability of all configurations decreases with increasing Mach number.

2. An increase in the nose fineness ratio of the trapezoidal-wing configuration decreases directional stability. Addition of a conical flare at the base of the triangular-wing model increases directional stability.

3. Addition of the conical flare to the triangular-wing configuration also increases longitudinal stability, lift, and drag. Lift-drag ratios are, however, reduced.

Ames Aeronautical Laboratory
National Advisory Committee for Aeronautics
Moffett Field, Calif., Jan. 6, 1956

REFERENCES

1. Penland, Jim A., Ridyard, Herbert W., and Fetterman, David E., Jr.: Lift, Drag, and Static Longitudinal Stability Data From an Exploratory Investigation at a Mach Number of 6.86 of an Airplane Configuration Having a Wing of Trapezoidal Plan Form. NACA RM L54I03b, 1955.

2. Ridyard, Herbert W., Fetterman, David E., Jr., and Penland, Jim A.: Static Lateral Stability Data From an Exploratory Investigation at a Mach Number of 6.86 of an Airplane Configuration Having a Wing of Trapezoidal Plan Form. NACA RM L55A21a, 1955.

3. Dunning, Robert W., and Ulmann, Edward F.: Static Longitudinal and Lateral Stability Data From an Exploratory Investigation at Mach Number 4.06 of an Airplane Configuration Having a Wing of Trapezoidal Plan Form. NACA RM L55A21, 1955.

4. Dunning, Robert W., and Ulmann, Edward F.: Exploratory Investigation at Mach Number 4.06 of an Airplane Configuration Having a Wing of Trapezoidal Plan Form. Longitudinal and Lateral Control Characteristics. NACA RM L55B28, 1955.

[redacted]

5. Neice, Stanford E., Wong, Thomas J., and Hermach, Charles A.: Lift, Drag, and Static Longitudinal Stability Characteristics of Four Airplane-Like Configurations at Mach Numbers from 3.00 to 6.28. NACA RM A55C24, 1955.

6. McLellan, Charles H.: A Method for Increasing the Effectiveness of Stabilizing Surfaces at High Supersonic Mach Numbers. NACA L54F21, 1954.

7. Eggers, A. J., Jr., and Syvertson, Clarence A.: Experimental Investigation of a Body Flare for Obtaining Pitch Stability and a Body Flap for Obtaining Pitch Control in Hypersonic Flight. NACA RM A54J13, 1955.

8. Eggers, A. J., Jr., and Nothwang, George J.: The Ames 10- by 14-Inch Supersonic Wind Tunnel. NACA TN 3095, 1954.

9. Dennis, David H., and Syvertson, Clarence A.: Effects of Boundary-Layer Separation on Normal Force and Center of Pressure of a Cone-Cylinder Model With a Large Base Flare at Mach Numbers From 3.00 to 6.28. NACA RM A55H09, 1955.

10. Savin, Raymond C., and Wong, Thomas J.: Lift, Drag, and Static Longitudinal Stability Characteristics of Configurations Consisting of Three Triangular Wing Panels and a Body of Equal Length at Mach Numbers From 3.00 to 6.28. NACA RM A55K21, 1956.

[redacted]

TABLE I.- STATIC DIRECTIONAL STABILITY CHARACTERISTICS OF THE FOUR CONFIGURATIONS TESTED; $\alpha = 0^\circ$

M	β	C_A	C_Y	C_n	M	β	C_A	C_Y	C_n	M	β	C_A	C_Y	C_n	M	β	C_A	C_Y	C_n
(a) Trapezoidal-wing model										(b) Modified trapezoidal-wing model									
3.00	-1.81	0.041	0.026	-0.0048	5.04	-1.84	0.036	0.019	-0.0013	3.00	-1.82	0.037	0.027	-0.0040	5.04	-1.84	0.033	0.020	-0.0003
	-.83	.041	.012	-.0024		-.91	.036	.010	-.0008		-.83	.037	.013	-.0020		-.91	.033	.010	-.0003
	.16	.041	-.002	.0002		.04	.036	0	.0001		.15	.036	-.001	.0003		.04	.033	0	0
	1.13	.040	-.017	.0032		.99	.036	-.010	.0011		1.13	.037	-.015	.0028		.99	.033	-.010	.0006
	2.10	.040	-.032	.0058		1.95	.036	-.021	.0024		2.11	.037	-.030	.0051		1.95	.033	-.021	.0012
	3.08	.041	-.046	.0082		2.90	.037	-.031	.0035		3.08	.037	-.044	.0073		2.90	.034	-.032	.0014
	4.06	.040	-.061	.0111		3.87	.037	-.041	.0040		4.07	.036	-.059	.0096		3.87	.034	-.042	.0015
4.26	-1.78	.036	.022	-.0029	6.28	-2.16	.044	.021	-.0013	4.26	-1.78	.032	.022	-.0022	6.28	-2.17	.043	.021	.0003
	-.90	.036	.011	-.0017		-1.14	.043	.011	-.0006		-.90	.032	.011	-.0010		-1.14	.039	.011	.0001
	0	.035	0	0		-.10	.043	.001	-.0001		0	.031	0	0		-.10	.038	.001	0
	.93	.036	-.012	.0019		.95	.043	-.008	.0004		.93	.032	-.011	.0012		.95	.039	-.009	.0002
	1.88	.036	-.023	.0035		2.01	.043	-.018	.0009		1.88	.032	-.023	.0025		2.01	.039	-.020	.0007
	2.84	.036	-.035	.0050		3.07	.043	-.029	.0020		2.85	.032	-.034	.0036		3.07	.040	-.031	.0010
	3.83	.036	-.046	.0064		4.13	.043	-.041	.0032		3.84	.032	-.046	.0045		4.13	.040	-.043	.0019
(c) Triangular-wing model										(d) Triangular-wing model with base flare									
3.00	-1.82	.030	.028	-.0043	5.04	-1.84	.026	.020	-.0004	3.00	-1.82	.034	.029	-.0059	5.04	-1.84	.029	.022	-.0024
	-.83	.030	.013	-.0020		-.91	.026	.010	-.0004		-.83	.034	.013	-.0028		-.91	.028	.011	-.0014
	.15	.029	-.001	.0003		.04	.026	0	0		.15	.033	-.002	.0004		.04	.028	0	0
	1.13	.029	-.015	.0028		.99	.026	-.011	.0010		1.13	.034	-.018	.0040		.98	.028	-.012	.0016
	2.11	.030	-.030	.0050		1.95	.026	-.021	.0014		2.11	.034	-.034	.0073		1.95	.029	-.023	.0028
	3.09	.030	-.045	.0072		2.91	.026	-.032	.0017		3.09	.034	-.050	.0104		2.91	.029	-.036	.0042
	4.08	.029	-.060	.0094		3.87	.026	-.044	.0022		4.08	.033	-.066	.0133		3.88	.029	-.048	.0051
4.26	-1.78	.025	.023	-.0022	6.28	-2.16	.033	.022	-.0003	4.26	-1.79	.028	.025	-.0037	6.28	-2.17	.034	.025	-.0031
	-.90	.025	.012	-.0010		-1.14	.032	.012	-.0002		-.90	.028	.012	-.0020		-1.14	.033	.013	-.0016
	0	.025	.001	-.0001		-.10	.032	.001	0		-.01	.028	0	0		-.10	.033	.002	-.0002
	.93	.025	-.011	.0013		.95	.032	-.008	0		.98	.028	-.014	.0024		.96	.033	-.012	.0018
	1.88	.025	-.023	.0028		2.01	.032	-.018	.0005		1.88	.028	-.027	.0049		2.01	.033	-.024	.0029
	2.85	.025	-.035	.0041		3.07	.032	-.031	.0017		2.85	.028	-.040	.0069		3.07	.034	-.036	.0035
	3.84	.025	-.047	.0049		4.14	.032	-.046	.0042		3.85	.028	-.053	.0087		4.14	.034	-.050	.0054

TABLE II.- STATIC LONGITUDINAL STABILITY CHARACTERISTICS OF THE TRIANGULAR-WING MODEL WITH BASE FLARE

M	α	C_L	C_D	C_m	x_{cp}
3.00	-0.94	-0.042	0.033	0.008	-0.19
	.03	-.004	.032	0	0
	1.02	.033	.033	-.010	-.31
	2.02	.070	.035	-.021	-.29
	4.04	.147	.043	-.043	-.28
4.26	-1.88	-.066	-.030	.018	-.27
	-.96	-.039	.029	.012	-.30
	-.02	-.010	.028	.004	-.45
	.95	.019	.028	-.003	-.15
	1.94	.048	.029	-.012	-.24
	2.96	.077	.032	-.020	-.25
	8.22	.224	.067	-.046	-.20
	10.19	.287	.089	-.058	-.19
	12.13	.346	.116	-.061	-.17
5.04	-1.89	-.054	.030	.007	-.12
	-.93	-.031	.028	.002	-.08
	.03	-.009	.027	-.001	.11
	.99	.014	.027	-.004	-.30
	1.98	.037	.028	-.008	-.22
	2.95	.062	.030	-.014	-.21
	7.25	.172	.052	-.030	-.17
	8.20	.199	.060	-.034	-.17
	9.16	.230	.069	-.041	-.17
	10.12	.260	.080	-.046	-.17
	11.08	.292	.091	-.052	-.17
	12.05	.325	.105	-.060	-.18
6.28	-2.19	-.052	.037	.007	-.13
	-1.15	-.032	.034	.005	-.14
	-.11	-.011	.032	.002	-.21
	.95	.011	.032	-.001	-.06
	2.02	.034	.032	-.006	-.17
	3.09	.058	.034	-.012	-.20
	6.74	.141	.049	-.016	-.11
	7.77	.166	.057	-.022	-.13
	8.80	.192	.066	-.026	-.13
	9.84	.219	.076	-.031	-.13
	10.91	.248	.088	-.040	-.16
	11.97	.277	.101	-.051	-.17

[redacted]

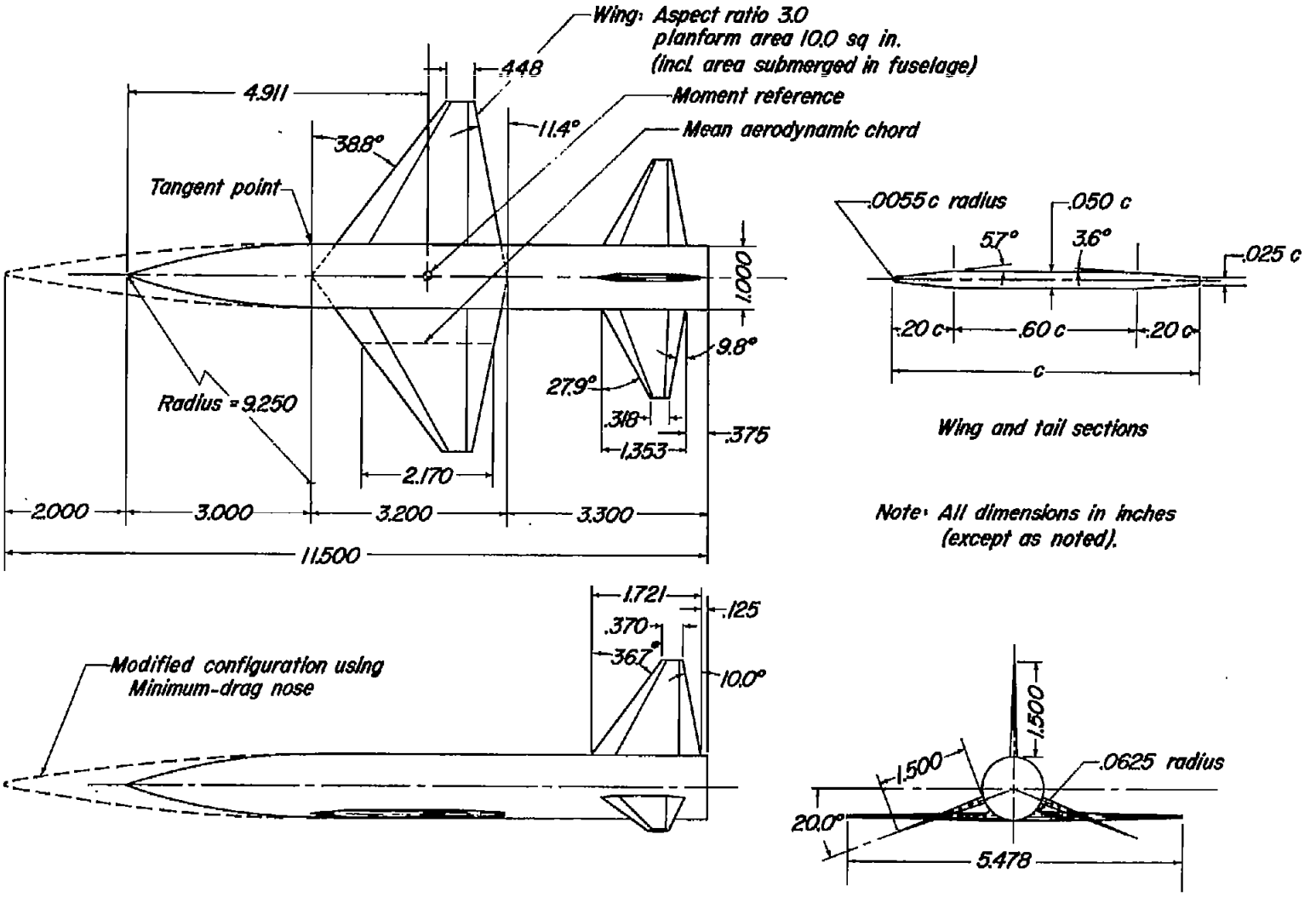

Figure 1.– Dimensions of trapezoidal-wing model.

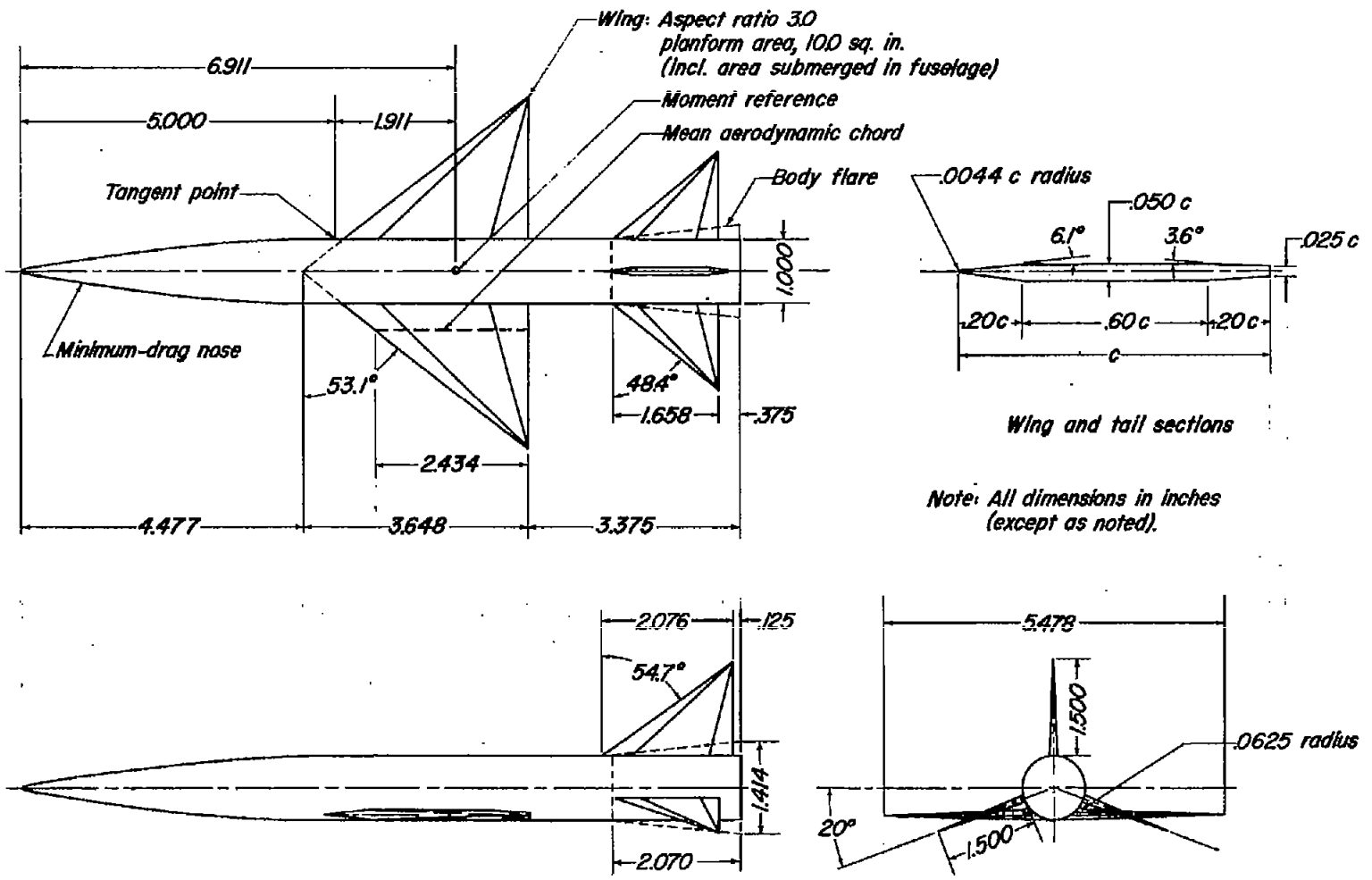

Figure 2.- Dimensions of triangular-wing model.

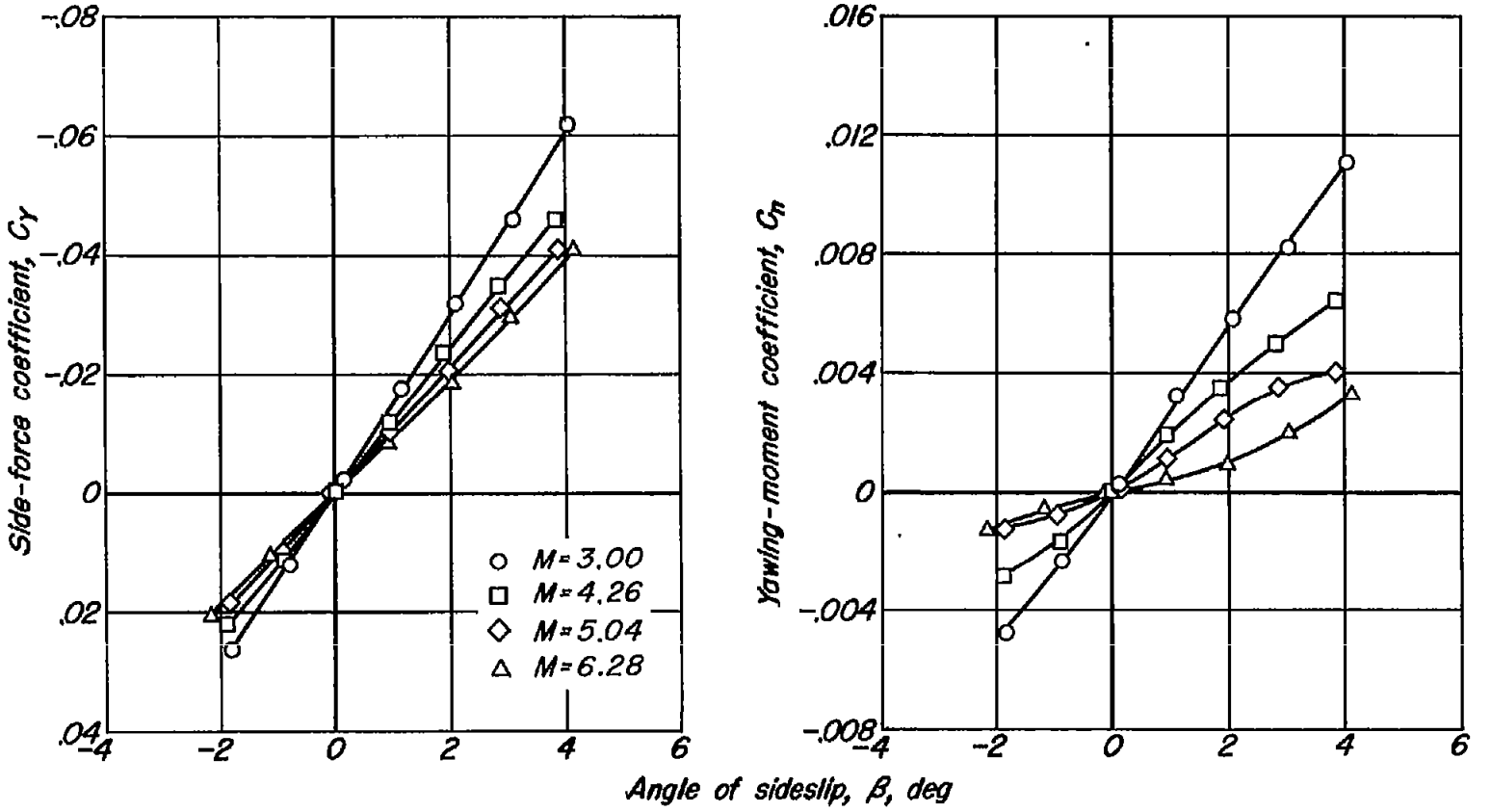

(a) Trapezoidal-wing model.

Figure 3.- Variation of side-force and yawing-moment coefficients with angle of sideslip, $\alpha = 0°$.

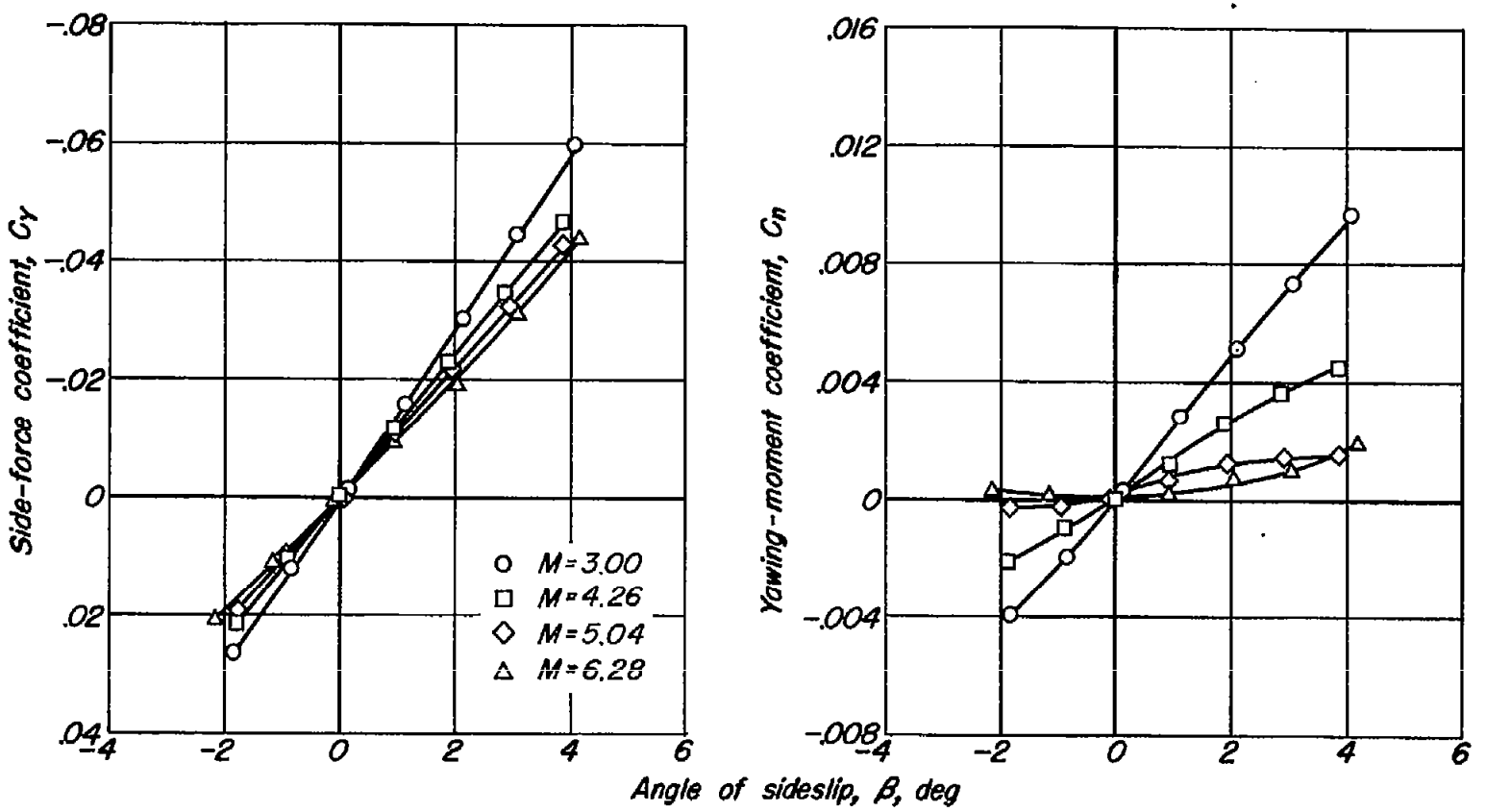

(b) Modified trapezoidal-wing model.

Figure 3.- Continued.

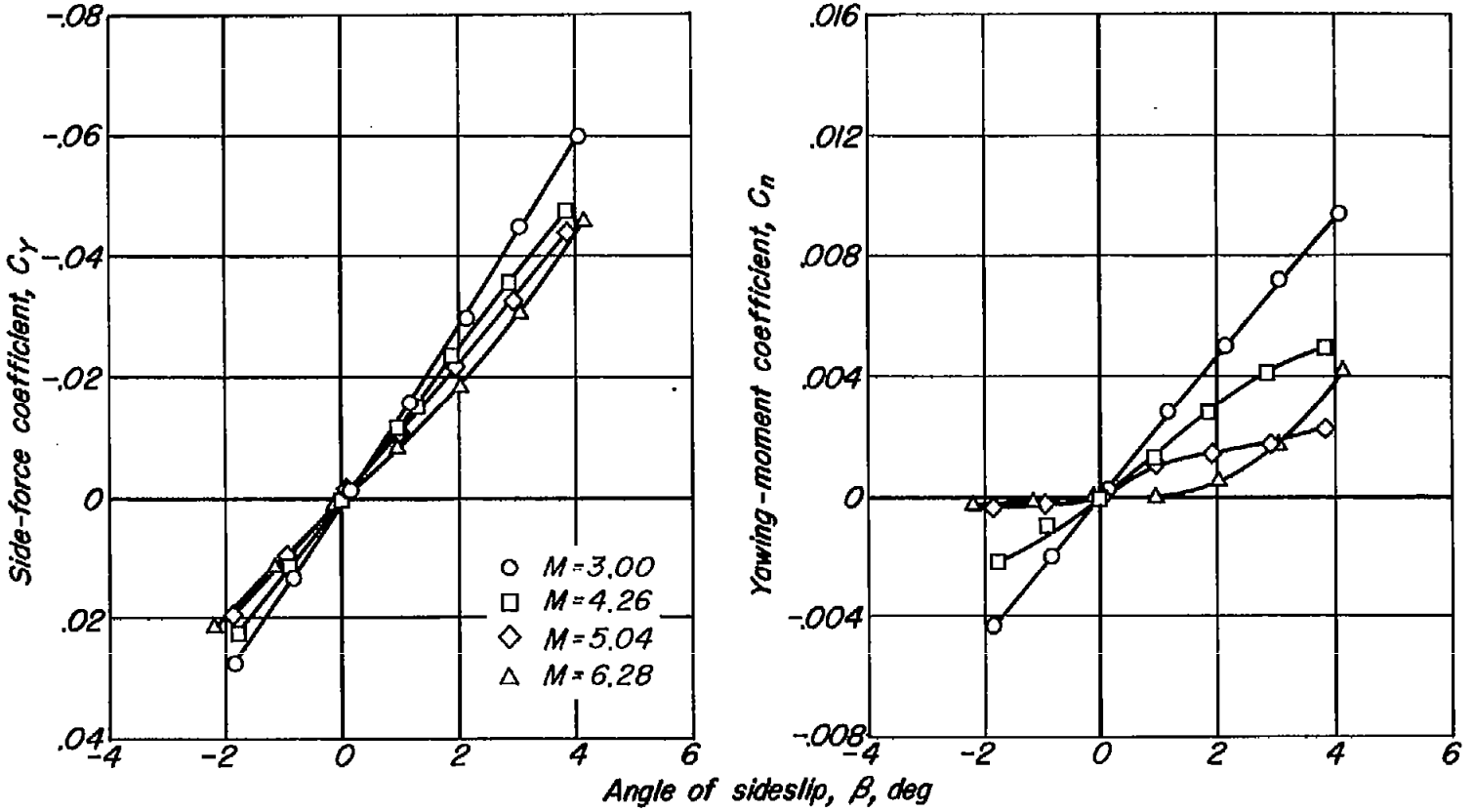

(c) Triangular-wing model.

Figure 3.- Continued.

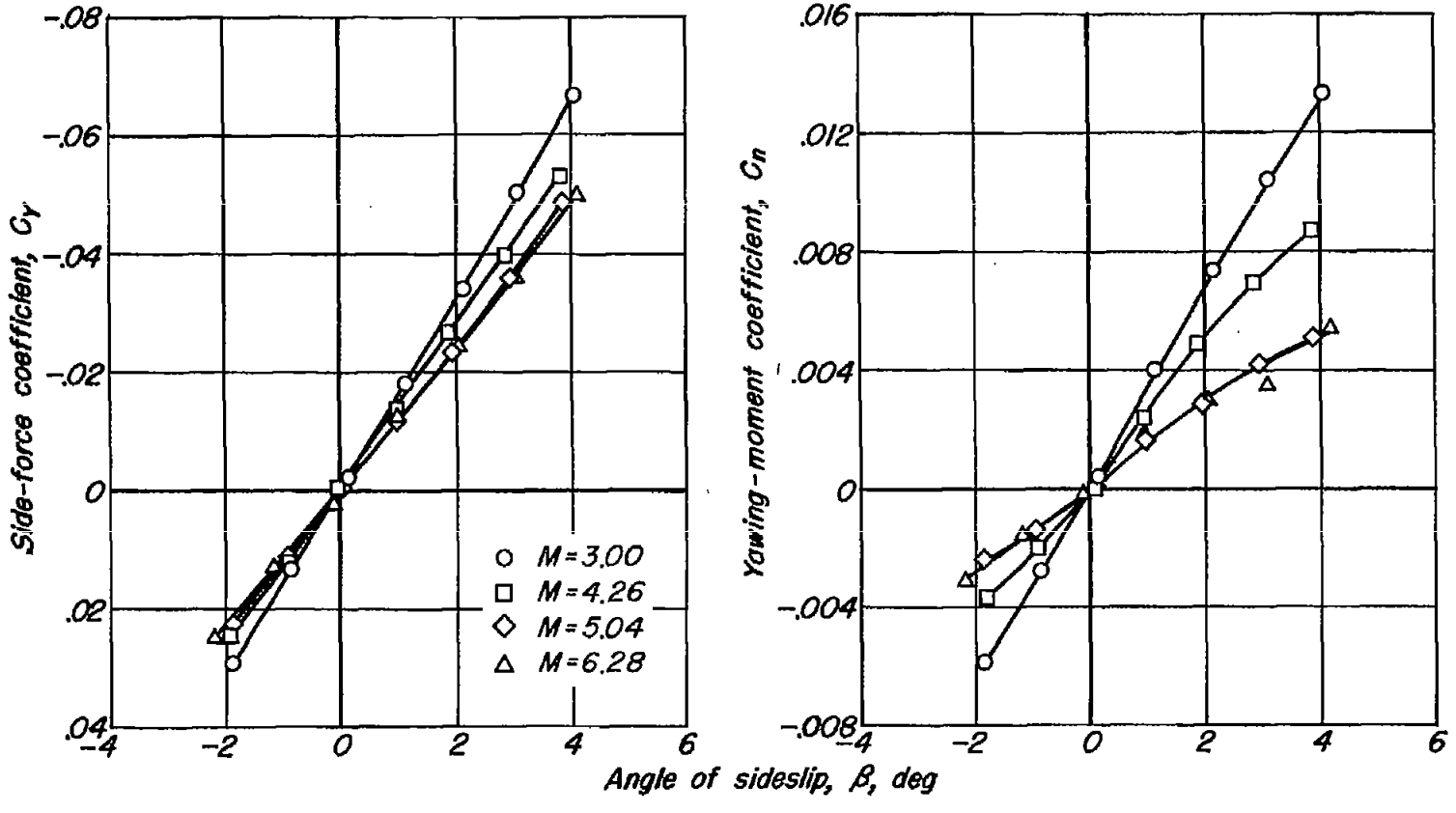

(d) Triangular-wing model with base flare.

Figure 3.- Concluded.

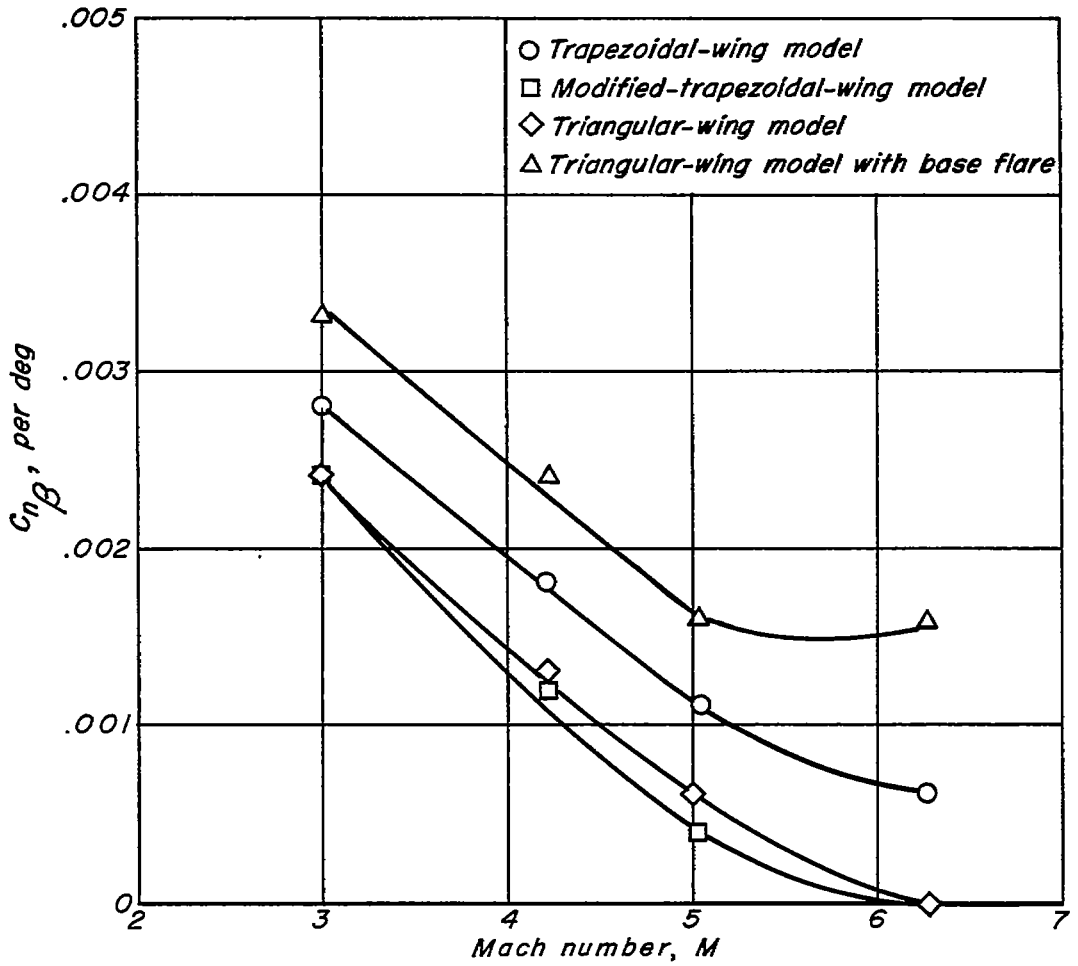

Figure 4.– Variation of directional stability with Mach number ($\alpha = \beta = 0°$).

[redacted]

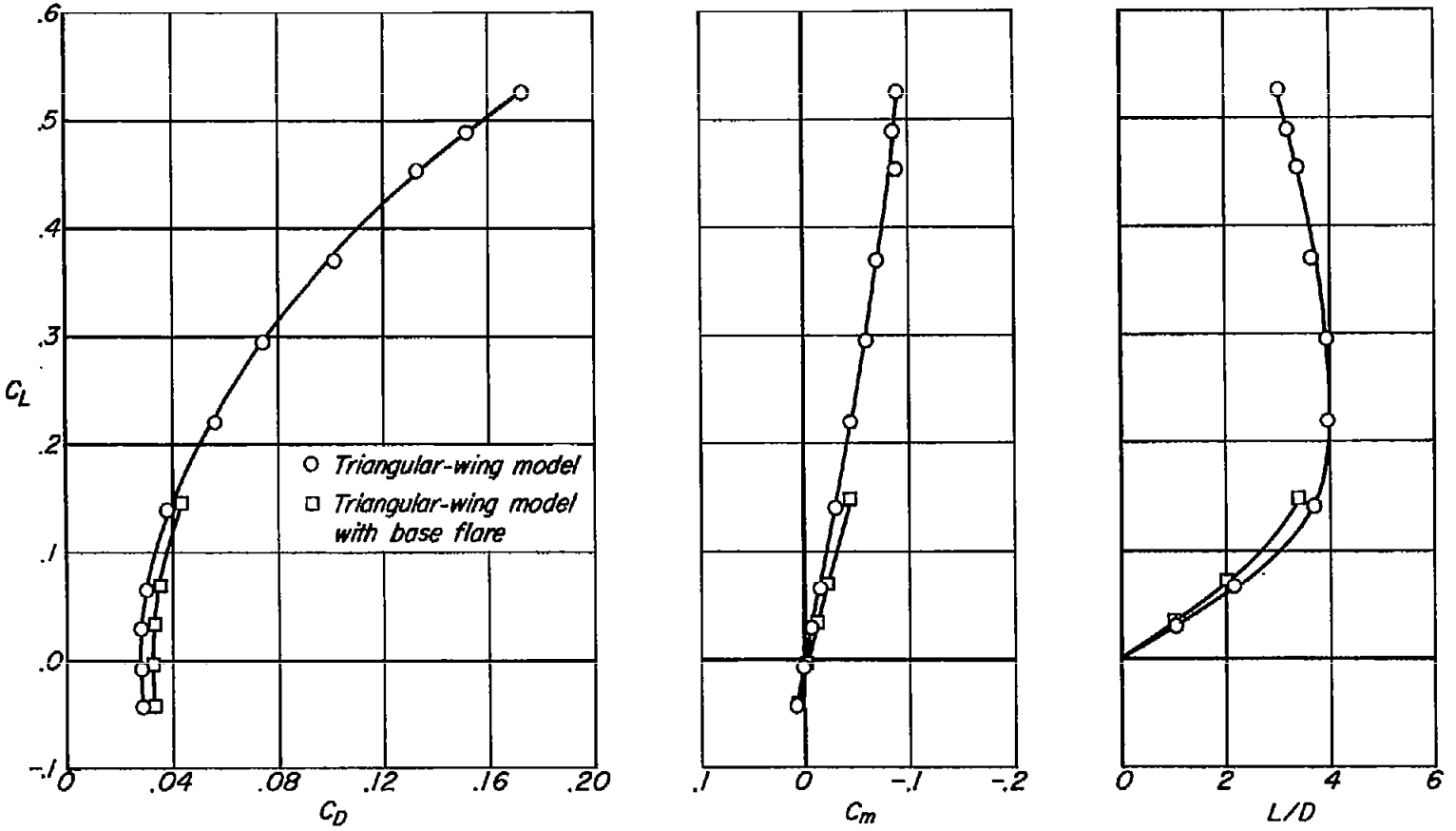

(a) M = 3.00

Figure 5.- Lift, drag, and static-longitudinal-stability characteristics of the triangular-wing models.

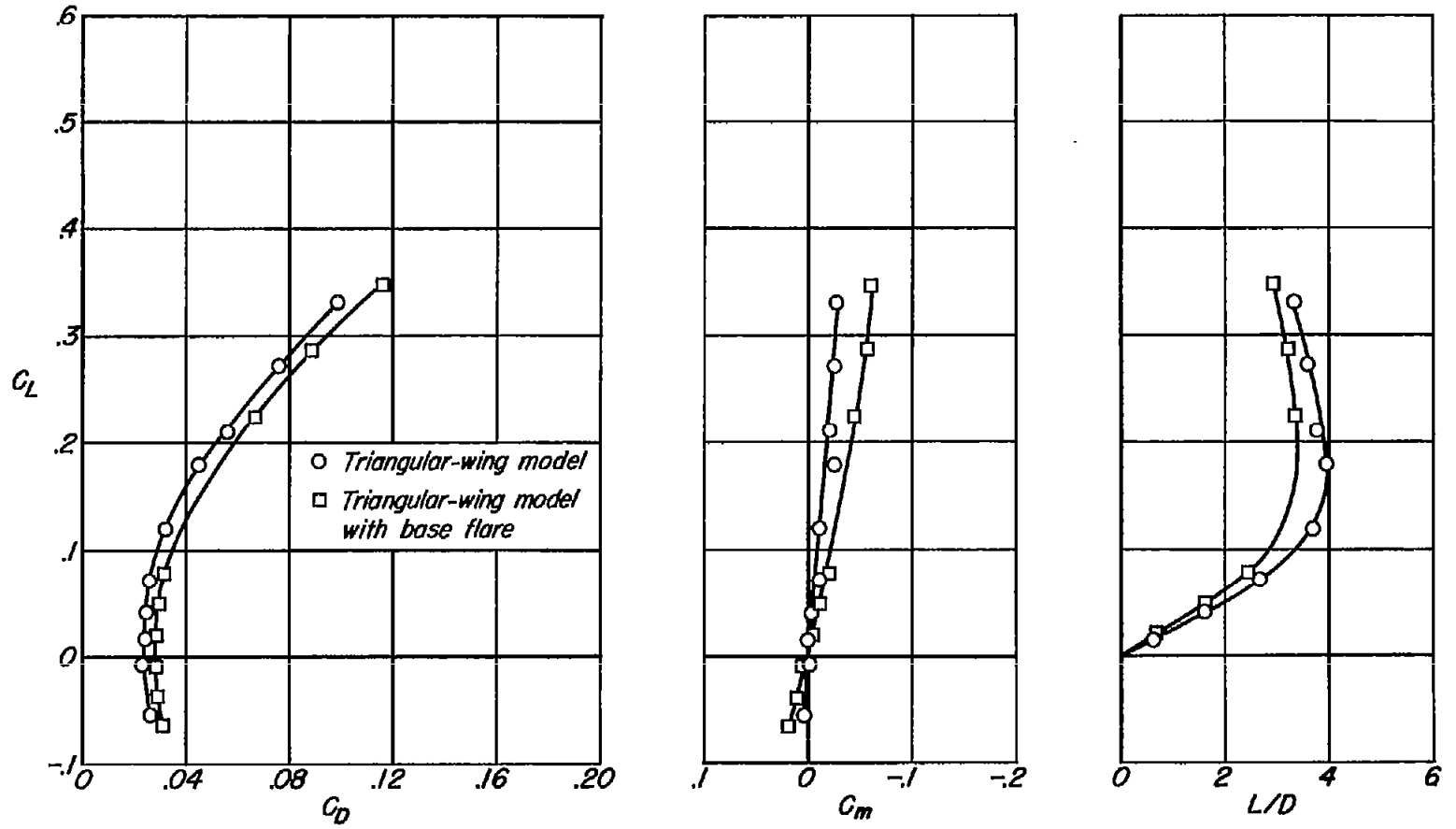

(b) M = 4.26

Figure 5.- Continued.

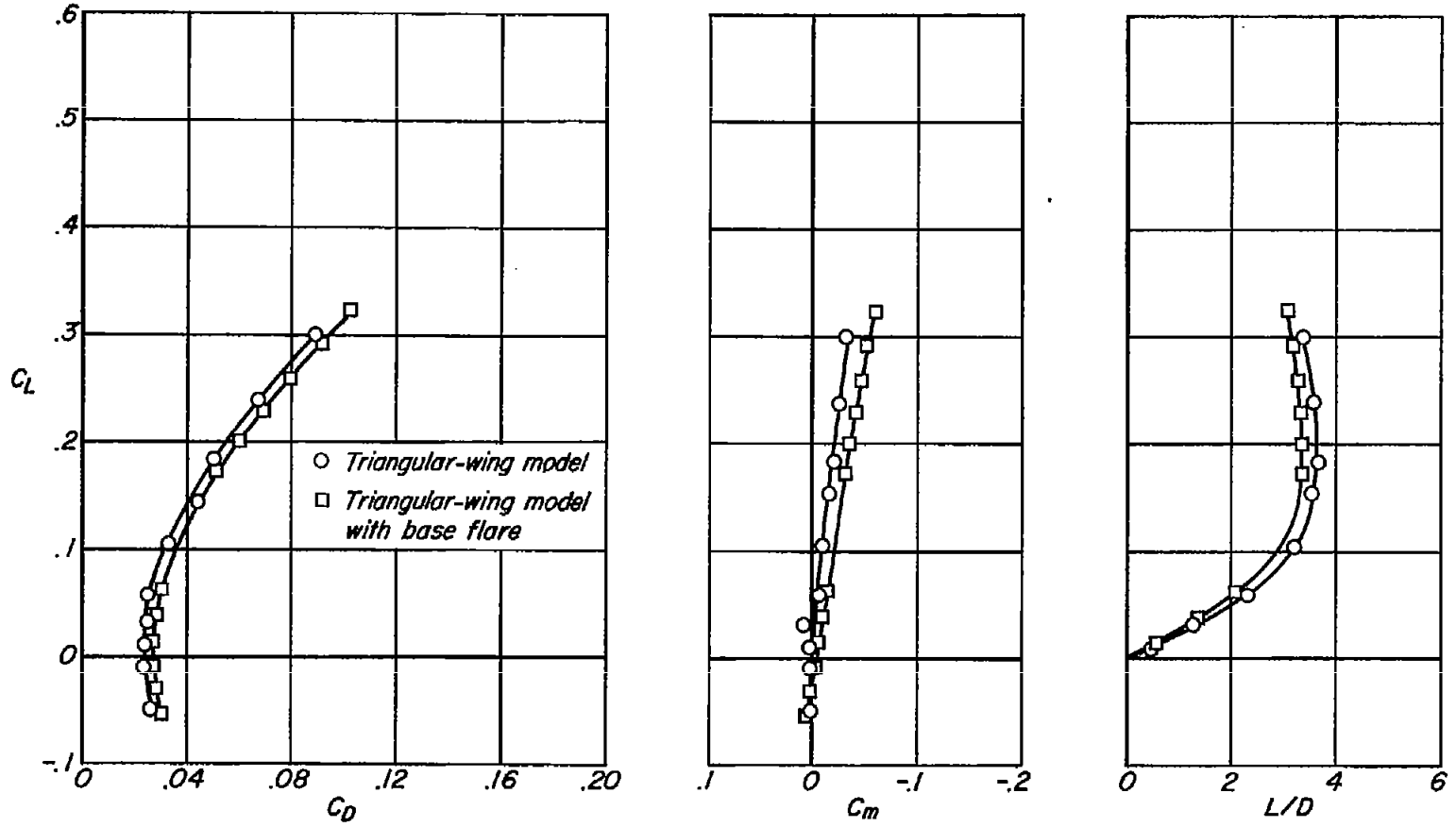

(c) M=5.04

Figure 5.- Continued.

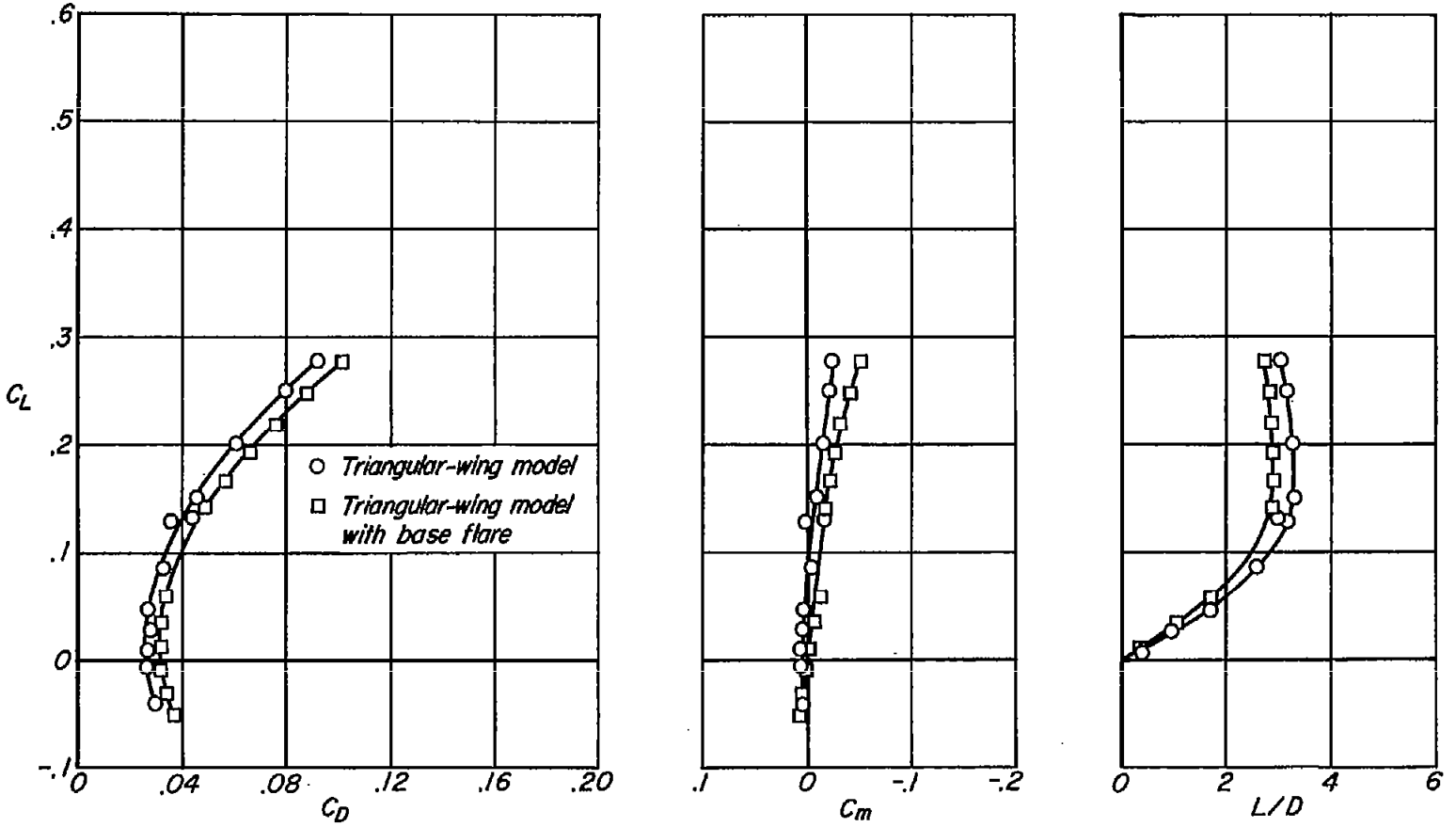

(d) M = 6.28

Figure 5.- Concluded.

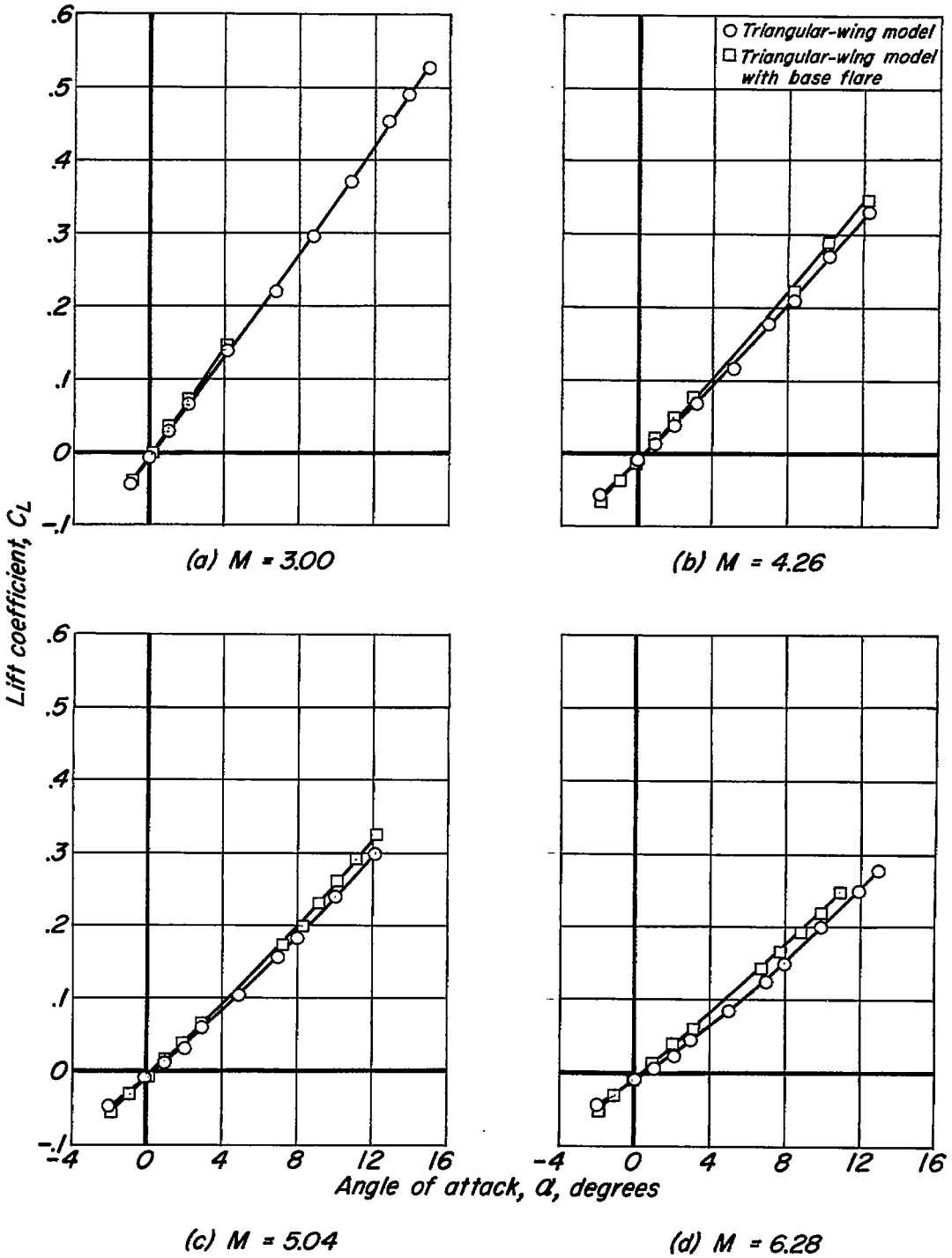

Figure 6.– Variation of lift coefficient with angle of attack for triangular-wing models.

[redacted]

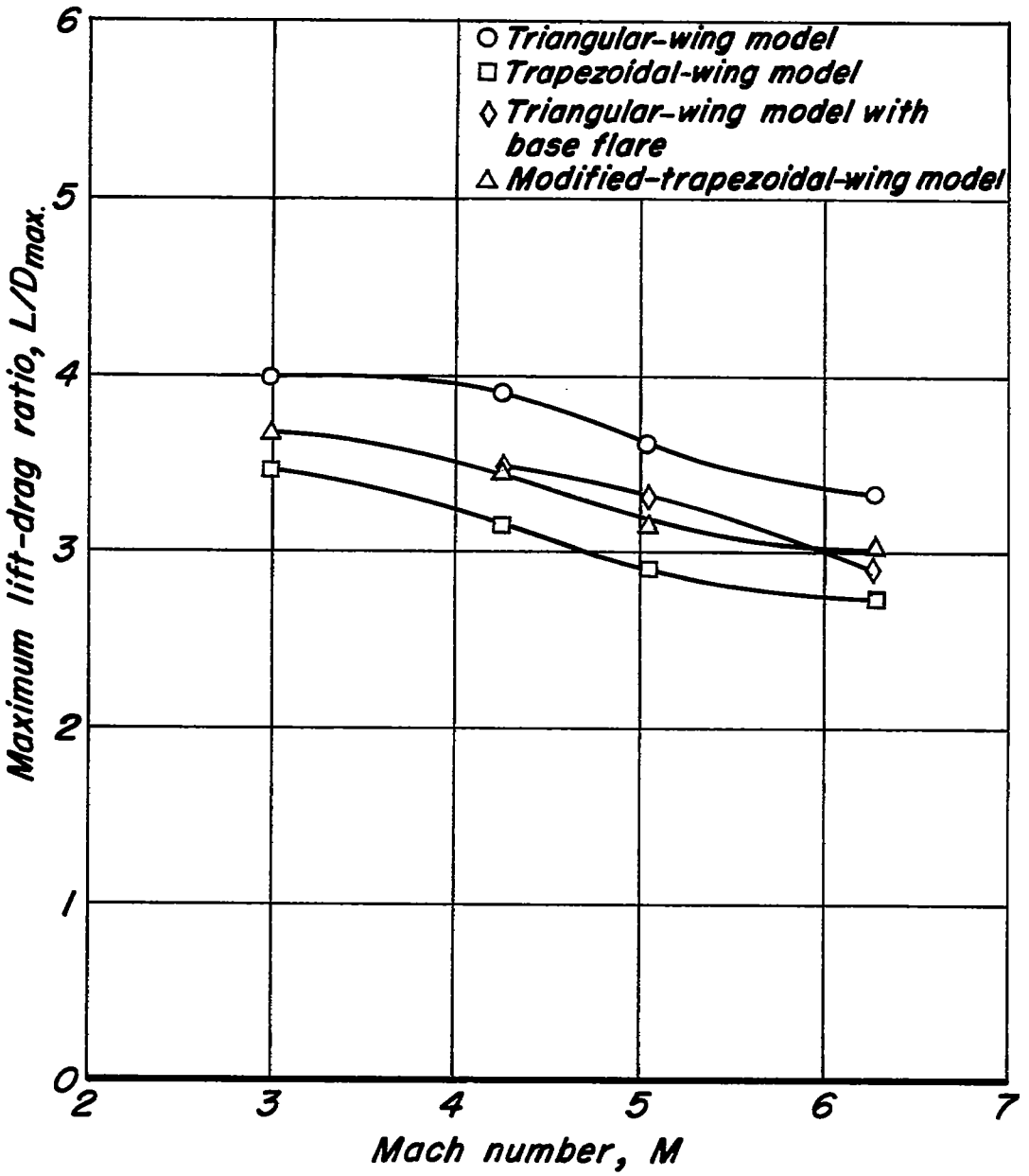

Figure 7.- Variation of maximum lift-drag ratio with Mach number for all models.

[redacted]